IRAS SOURCES ASSOCIATED WITH SMALL NEBULAE IN STAR FORMING REGIONS: OPTICAL AND NEAR INFRARED IMAGES[1]

MAURICIO TAPIA
Instituto de Astronomía, UNAM, Apartado Postal 877, Ensenada, 22830, B.C., Mexico
Electronic mail: mt@bufadora.astrosen.unam.mx

PAOLO PERSI
Istituto Astrofisica Spaziale, CNR, CP 67, 00044 Frascati, Italy
Electronic mail: persi@saturn.ias.fra.cnr.it

JOAQUÍN BOHIGAS
Instituto de Astronomía, UNAM, Apartado Postal 877, Ensenada, 22830, B.C., Mexico
Electronic mail: jbb@bufadora.astrosen.unam.mx

MARCO FERRARI-TONIOLO
Istituto Astrofisica Spaziale, CNR, CP 67, 00044 Frascati, Italy
Electronic mail: ferrari@saturn.ias.fra.cnr.it

Received 1996 November 27; revised 1997 February 18

ABSTRACT

Optical CCD and near-IR broad and narrow-band imaging have been obtained of a sample of 11 small optical nebula associated with *IRAS* sources in star forming regions in order to perform a morphological and photometric study. More than 130 sources were detected in K. The $J-H$ versus $H-K$ diagram was used to establish their nature. The most massive regions, Gy 2-18, Gy 4-2, and Gy 3-7, have embedded clusters of early-type stars and their associated nebulae were found to be photoionized. The *IRAS* sources in L1455, L1473, L1165 and Gy 4-1 with near-IR reflection nebulae were found to be Class I young stellar objects with associated molecular outflows. The results for each region is discussed in detail. [S0004-6256(97)04505-6]

1. INTRODUCTION

An important tool used to examine and identify regions with active stellar formation, is to study isolated red nebulosities, with morphologies resembling cometary nebulae or Herbig–Haro objects within and in the vicinity of dark regions with far-IR sources. Lists of these nebulae have been reported by Gyulbudaghian *et al.* (1978; GGD), Parsamian & Petrosian (1979; PP), Gyulbudaghian (1983; Gy 2), Gyulbudaghian (1984a; Gy 3), and Gyulbudaghian (1984b; Gy 4); all compiled in a list of "Herbig-Haro-Like objects found at Byurakan Observatory" (Gyulbudaghian *et al.* 1987; HHL). This name is unfortunately misleading, insofar as it associates the nebulae *a priori* with a particular physical process, i.e., shocks, a possibility amongst various. In a CO ($J=1-0$) survey conducted on a large sample of nebulosities contained in these lists (98 objects), it was found that over 80% of them are associated with molecular clouds (Torrelles *et al.* 1983). On the other hand, using a smaller sample of these objects, Persi *et al.* (1988a) found that approximately 50% are also close to an *IRAS* source. More recently, Persi *et al.* (1994) searched for H_2O 22.2 GHz maser emission from 68 red peculiar nebulosities, concluding that YSOs with nebulosities are more likely to host water vapor masers.

Thus, lists of these red nebulosities can be used as a starting point in order to carry out research on various facets of the stellar formation problem. As an example, Persi *et al.* (1988b) studied in the near-IR a set of nebulosities associated with *IRAS* sources and discovered new young stellar objects at different evolutionary stages by inspecting their near to far-infrared energy distributions. In this work we selected a group of red nebulosities associated to *IRAS* sources from the aforementioned works, which upon inspection of their *IRAS* colors, are likely to be related to the formation of stars in various mass ranges. Four of these nebulae (PP 9, PP 13, Gy 2-21, and Gy 2-13, located within dark clouds L1455, L1473, and L1165, respectively) are probably associated to low mass star formation. The large IR luminosity of the *IRAS* sources associated to Gy 4-2 and Gy 3-7, suggests that massive stars are being formed in these regions whereas Gy 2-18 and Gy 4-1 are probably related to the formation of intermediate mass stars. Therefore, different aspects of star formation in the three major regions of the stellar mass spectrum, such as evolutionary and ambient medium effects or likelihood of cluster formation, can be explored with this sample.

We have obtained optical and near–IR images of the re-

[1]Based on observations collected at the Observatorio Astronómico Nacional at San Pedro Mártir, Las Campanas Observatory, Telescopio Infrarosso del Gonergrat and European Southern Observatory.

TABLE 1. Log of optical observations and integration times (minutes).

Name	α 1950 δ	Run	Continuum	Hα	[S II]6724	I_c
PP 9	$3^h24^m43\overset{s}{.}3+30°01'43''$	SPM90	20	20[a]	20	20
GGD 2	$3^h25^m29\overset{s}{.}9+30°50'31''$	SPM95	···	40	20	10
HH 14	$3^h25^m44\overset{s}{.}2+30°50'23''$	SPM95	20	40	40	40
PP 11	$3^h50^m47\overset{s}{.}2+38°01'51''$	SPM90	20	20[a]	···	20
PP 13	$4^h07^m21\overset{s}{.}2+38°00'08''$	SPM90	20	40[a]	40	15
Gy 2-13	$4^h59^m06\overset{s}{.}6-08°56'32''$	SPM90	20	40[a]	···	15
Gy 2-18	$5^h43^m59\overset{s}{.}7+30°35'09''$	SPM95	40	40	40	20
Gy 4-1	$6^h24^m57\overset{s}{.}1-10°07'33''$	SPM91	20	20	···	10
Gy 4-2	$6^h56^m47\overset{s}{.}4-03°55'24''$	SPM90,91	20	20[a]	···	6
Gy 3-7	$7^h06^m59\overset{s}{.}0-10°45'32''$	SPM91	20	20	20	···
Gy 2-21	$22^h05^m09\overset{s}{.}6+58°48'06''$	SPM90,91,95	20	40	20	20

[a]Includes the [N II]6548,6584 Å lines.
SPM90: 2.1 m tel., CCD 384×576, 8–11 Nov 1990.
SPM91: 2.1 m tel., CCD 384×576, rebinned 2×2, 26–30 Nov 1991.
SPM95: 1.5 m tel., CCD 1024×1024, 28–30 Nov. 1995.

gions using both narrow and broad band interference filters as the combination of optical and near–IR images provides a proven method to investigate the nature of young stellar objects and their interactions with the ambient medium (e.g., Bohigas *et al.* 1993). Observations are described in Sec. 2, while in Sec. 3 the results and discussion for each source are given separately. A summary of the conclusions is presented in Sec. 4. As there has been some confusion about the nomenclature of the nebulae under study, we give ample cross-references following the acronyms used by SIMBAD.

2. OBSERVATIONS

2.1 Optical Images

Optical images were obtained on 1990 November and 1991, with the 2.1 m *f*/7.5 telescope, and 1995 October with the 1.5 m *f*/13.5 telescope, of the Observatorio Astronómico Nacional at San Pedro Mártir, B.C., Mexico. A Thomson CHFTH7883 384 ×576 pixel CCD, with a plate scale of 0.30″/pixel, rebinned 2×2 at read-out, was used in the first two runs (SPM90, SPM91). Image quality, measured by the FWHM of stars, was ~1.5″ during these runs. A Thomson TH31156 1024 ×1024 Metachrome II coated CCD detector, with a plate scale of 0.20″/pixel, was used in the 1995 run (SPM95). In this case, image quality was ~1.2″. Data reduction was carried out with IRAF.[2] A detailed log of these observations is presented in Table 1. Continuum images were taken either with a 102 Å FWHM filter centered at 6459 Å, or a 51 Å FWHM filter centered at 6253 Å. The Hα image was obtained either with an 11 Å FWHM filter centered at 6564 Å, or with an 89 Å FWHM filter centered at 6607 Å (which included the [N II] lines at 6548 and 6584 Å). Finally, the image for the S^+ lines at 6717 and 6731 Å was obtained with a 52 Å FWHM filter centered at 6729 Å. Images of the region were also taken with an I_c filter. In the case of the narrow-band images and in spite of the fact that no absolute calibration was feasible, relative calibration of the source frames was performed by matching the field star counts once the sky background was removed. Then, we compared the continuum-subtracted Hα and [S II] 6724 Å frames in order to discern reflection from emission nebulae and, in the latter case, to establish whether the gas is photoionized or shock-excited. For pairs of lines whose wavelengths are relatively close, as in this case, this procedure is adequate to produce approximate but reliable line ratios even with the non-uniform atmospheric conditions that we had during and between the three runs (non photometric weather prevailed during the first two runs and part of the third). As is well known, both observationally and theoretically (e.g., Hartigan *et al.* 1987; Cantó 1981), when the ratio [S II] 6724/Hα>0.5, shocks are the predominant excitation mechanism.

[2]IRAF is distributed by NOAO which is operated by AURA under contract to the NSF.

2.2 Near-Infrared Images

The infrared images were obtained during four runs, ESO92, LCO93, TIRGO, and SPM95, at different observatories in four consecutive years. The log of the IR observations is presented in Table 2.

The ESO92 observations were carried out with the IRAC–1 near-IR camera at the 2.2 m ESO/MPI telescope on the nights of 1992 January 20–22. The camera used a HgCdTe 64×64 array from Phillips Components Ltd., with a plate scale of 0.8″/pixel. These were used for measurements in the *L* band only.

The LCO93 observations were made on the nights of 1993 November 30 and December 1 with the LCO Near-Infrared Camera (Persson *et al.* 1992) on the 2.5m DuPont telescope under sub-arcsec seeing. The camera has a NICMOS3 256×256 HgCdTe detector and the scale was 0.35″/pixel.

The NICMOS3 camera ARNICA (Lisi *et al.* 1996) with a plate scale of 0.95″/pixel was used on the nights of 1994 February 13–16 for the observations at the 1.5 m Italian infrared telescope of Gornergrat (TIRGO).

The SPM95 observations were obtained on the nights 1995 December 7–10 with the NICMOS3-based SPM Infrared Camera, CAMILA (Cruz-González *et al.* 1994) attached to the 2.1 m telescope of the Observatorio Astronómico Nacional at San Pedro Mártir in the *f*/13.5 configuration in

TABLE 2. Log of IR observations and integration times (s).

Name	Run	*J*	*H*	*K*	*L*	H_2	Brγ	Cont.
PP 9	SPM95	450	360	180	···	···	···	···
L1455FIR	SPM95	540	450	540	···	600	···	···
GGD 2	SPM95	320	320	320	···	···	···	···
HH 14	SPM95	240	160	320	···	720	···	280
PP 11	TIRGO	60	60	60	···	240	···	···
PP 13	TIRGO	60	60	60	···	240	···	···
Gy 2-13	ESO92	180	180	180	···	···	···	···
Gy 2-18	SPM95	240	200	120	···	640	···	160
Gy 4-1	LCO93	480	480	480	···	···	720	240
	ESO92	···	···	···	330	···	···	···
Gy 4-2	LCO93	480	480	480	···	···	720	240
Gy 3-7	SPM95	360	300	120	···	400	···	···
	ESO92	···	···	···	330	···	···	···
Gy 2-21	SPM95	540	450	270	···	600	···	···

ESO92: 2.2 m tel., IRCAM1, 20–22 Jan. 1992.
LCO93: 2.5 m tel., LCO-NICMOS, 7–10 Dec. 1993.
TIRGO: 1.5 m tel., ARNICA, 13–16 Feb. 1994.
SPM95: 2.1 m tel., CAMILA, 7–10 Dec. 1995.

direct mode with a cold stop. The plate scale was 0.48″/pixel and the FWHM of stars during the four nights was systematically below one arcsec, a feature which has become possible only recently due to the new active mirror support system in this telescope (Salas *et al.* 1996).

The filters used in LCO and SPM were the normal *J* and *H*, while the *K* filter was the so-called short-*K* ($\lambda_0=2.125$ μm, $\Delta\lambda=0.35$ μm). In SPM the H_2 filter was defined by $\lambda_0=2.122$ μm $\Delta\lambda=0.02$ μm, the Brγ at 2.17 μm and the continumm filter by $\lambda_0=2.26$ $\Delta\lambda=0.06$, avoiding the brightest H_2 lines and the Brγ line.

In all cases, each individual frame was reduced by sky subtracting and flat fielding using the median of several images taken in the immediate vicinity of the region, some of them also including the program object in different positions to increase the on-source integration time and at the same time, increasing the covered area (by way of mosaicing). As shown in Table 2, the sources Gy 2-18, Gy 4-1, Gy 4-2, and Gy 3-7 have been observed with different telescopes. For these, we only took into account images taken during the runs SPM95 and LCO93 because they are of better quality.

Stellar photometry was performed with DAOPHOT (Stetson 1987) within IRAF, with apertures according to the quality of the images in each run. These were, 3″ for SPM95 and LCO93, 4″ for ESO92, 8″ for PP 11 and 15″ for PP 13 (both at TIRGO) For the broad-band images, flux calibration was done by observing standards from the list of Elias *et al.* (1982) and UKIRT (Users Manual) list of faint standards. The internal errors are estimated to be within 5% but absolute errors are believed to be larger, as no color corrections were made. In only a few cases, confusion may render the photometry unreliable and this possibility was monitored and corrected individually for critical sources only (e.g., in the compact trapezium system at the center of Gy 4-2).

Figures 1 to 11 show the broad- and narrow-band optical and near-infrared images centered in the position of the *IRAS* sources or associated nebulosities, as indicated in the respective caption.

3. RESULTS AND DISCUSSION

A total of 133 sources were detected in the *K*-band with a S/N$\geqslant$10, of which approximately 70% were measured also in *J* and *H*. The astrometry was obtained with an accuracy of 1″–2″ using the GSC and the digitized Palomar Sky Survey. Identification charts are provided in Fig. 12. The colors of all the sources found are plotted in the $J-H$ versus $H-K$ diagrams shown in Fig. 13. As seen in these two-color plots, a significative number of sources show infrared excesses, indicating the presence of very young stellar objects (YSOs). Table 3 gives the photometry and positions of sources which are probably related to the star forming region, that is, those *not* displaying colors typical of reddened late-type stars as well as the very red objects detected only in *K* or with $H-K\geqslant 1.8$. Spectral energy distributions of the *IRAS* sources and their near-infrared conterparts were analyzed and their near-infrared spectral indexes

$$n_{2-25\,\mu\mathrm{m}}=\frac{d\,\log(\nu F_\nu)}{d\,\log\,\nu}$$

were computed. Based on these, the YSOs were classified according to the evolutionary scheme proposed by Adams *et al.* (1987) (see also revision by, e.g., André 1994) which assigns to Class I the youngest stellar objects in their late accretion phase and already detectable in the near-infrared, Class II to those with optically thick disks and collimated outflows and Class III to those with optically thin or no disk. The calculated total luminosities (at the assumed distances) were the bases for determining whether the YSOs are of low mass (T Tauri-type), intermediate mass (Herbig Ae/Be) or high mass (O-B2), the latter also supported by the presence of detectable H II regions.

3.1 PP 9 (GM 1-13, RNO 15) and L1455-FIR

We have imaged two different fields in this region. One centered on the faint red cometary-like nebula catalogued by

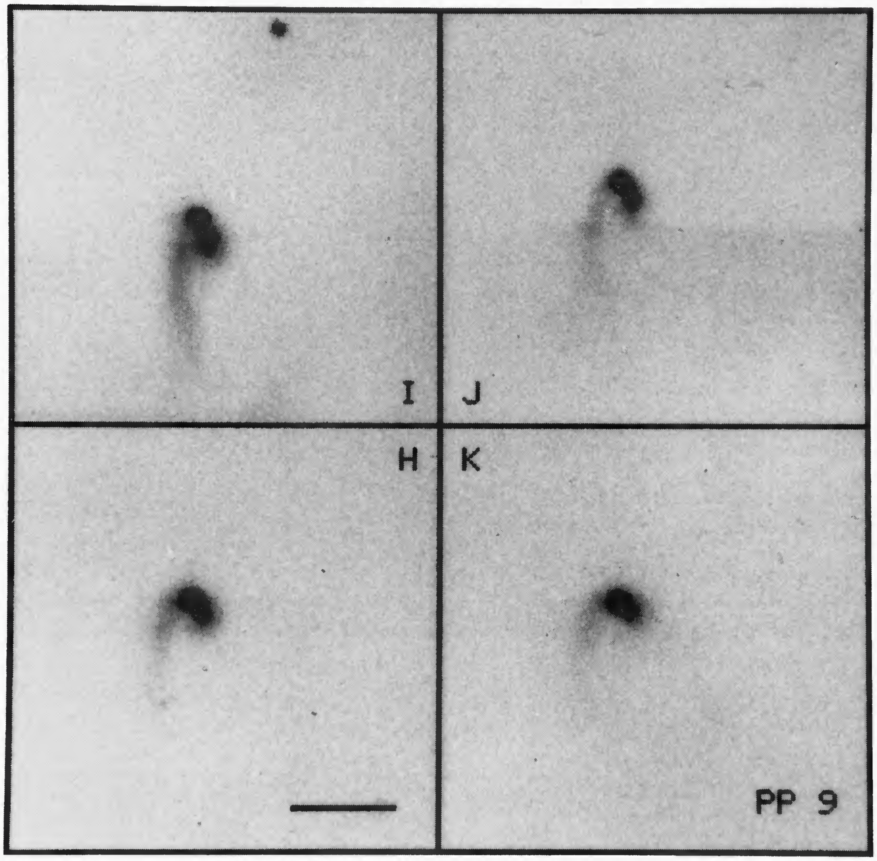

FIG. 1. *IJHK* images of PP 9. North is to the top, east to the left. The length of the bar is 30″.

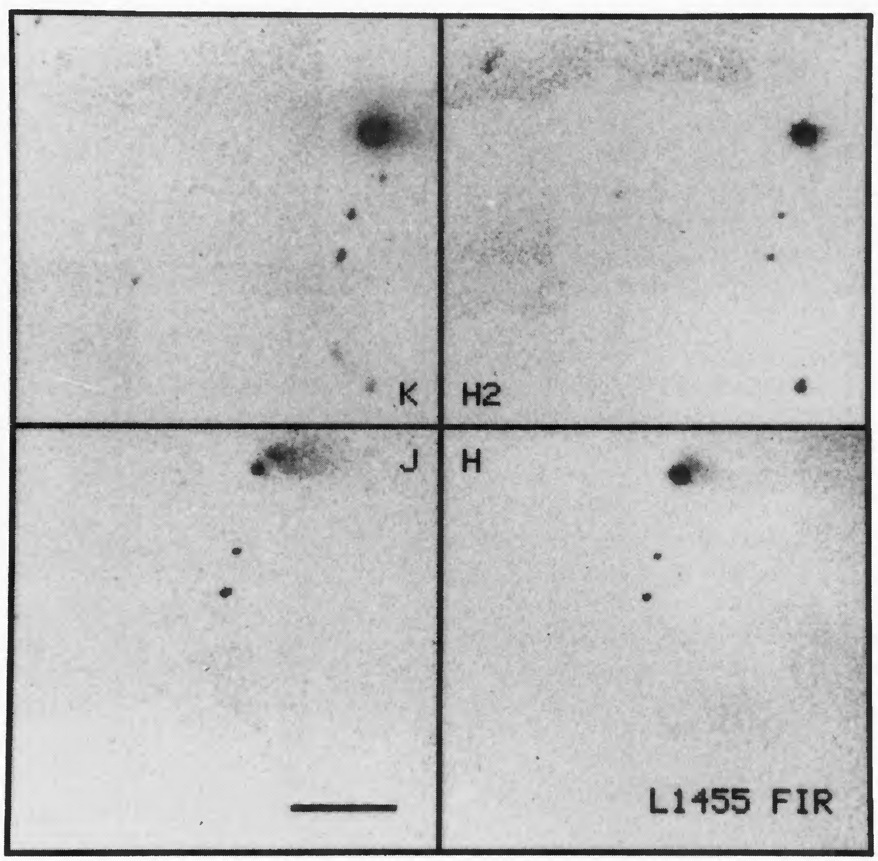

FIG. 2. *JHK* and H_2 images of L1455FIR. North is to the top, east to the left. The length of the bar is 30″.

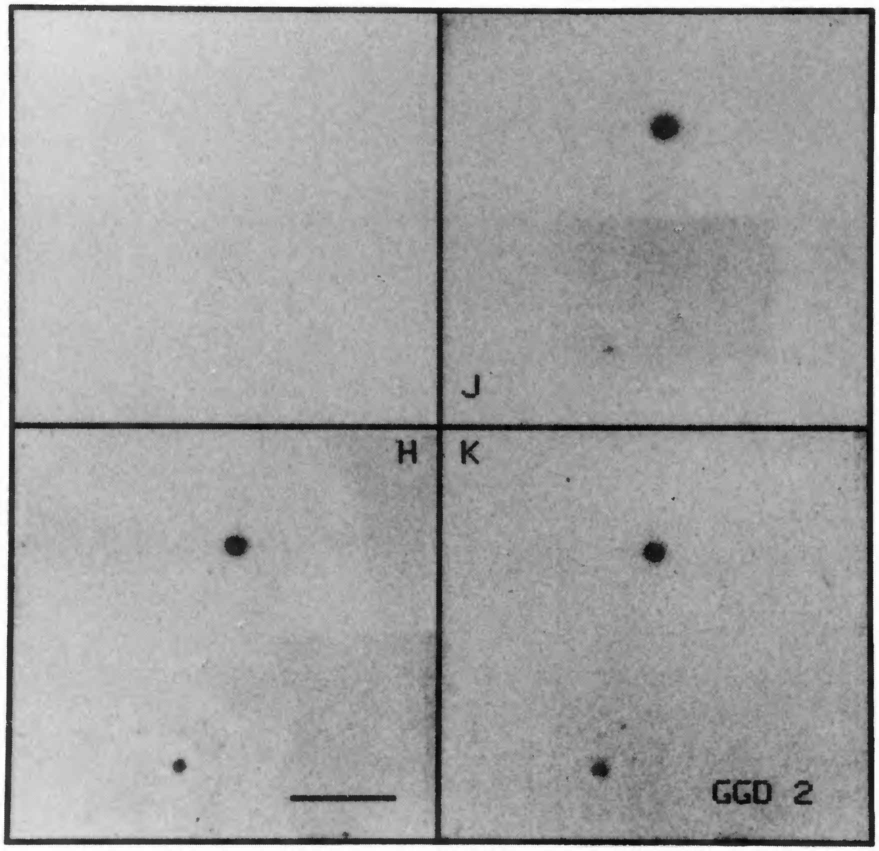

FIG. 3. *JHK* images of GGD 2. North is to the top, east to the left. The length of the bar is 30″.

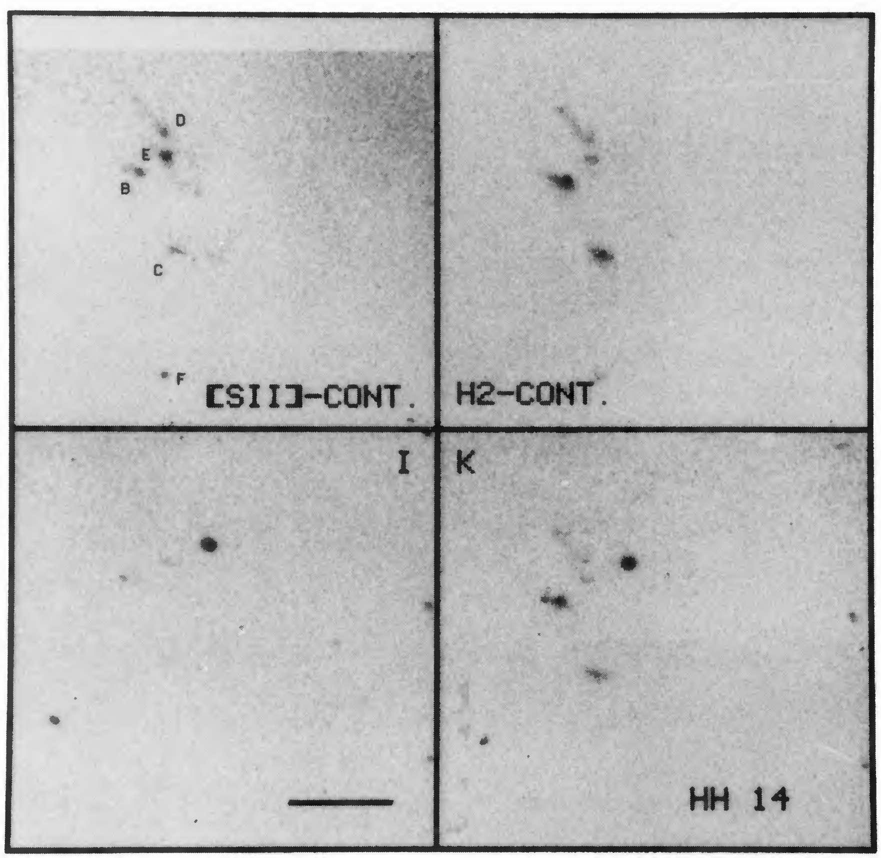

FIG. 4. *IK* and continuum subtracted [S II] 6724 Å and H_2 2.12 μm images of HH14. North is to the top, east to the left. The length of the bar is 30″.

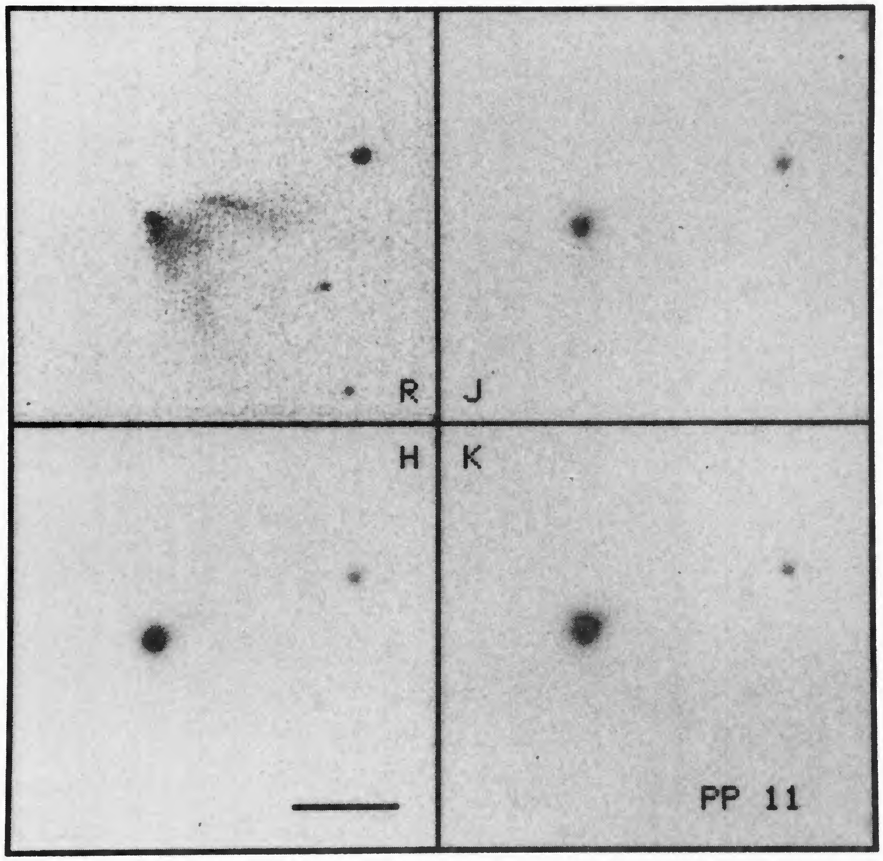

FIG. 5. *RJHK* images of PP 11. North is to the top, east to the left. The length of the bar is 40″.

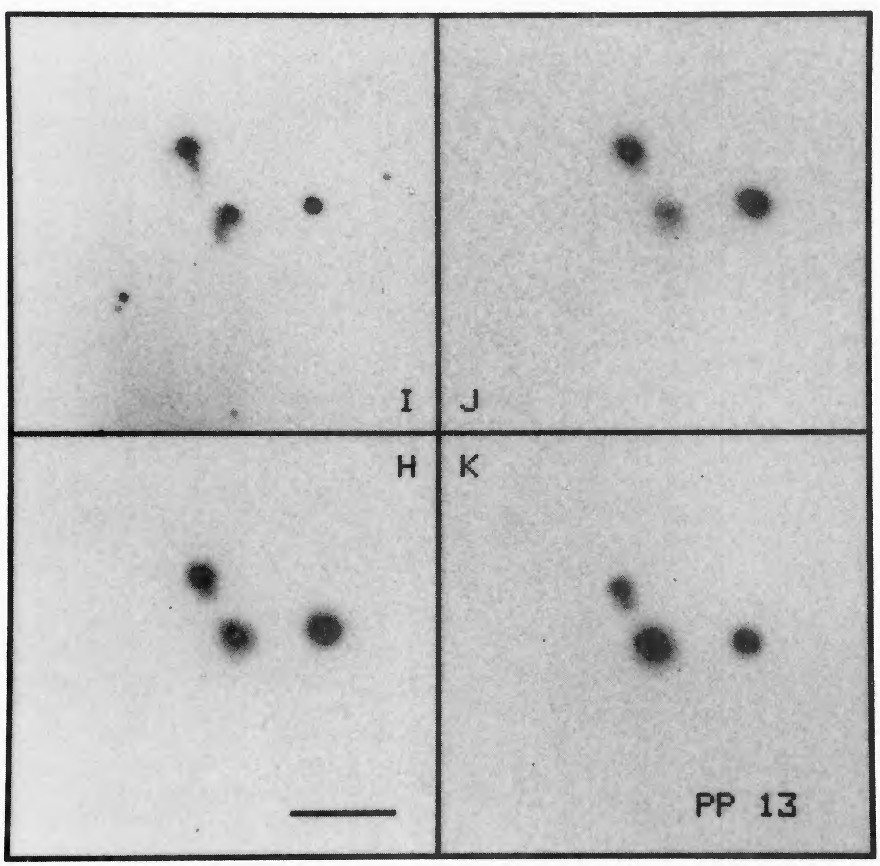

FIG. 6. *IJHK* images of PP13. North is to the top, east to the left. The length of the bar is 30″.

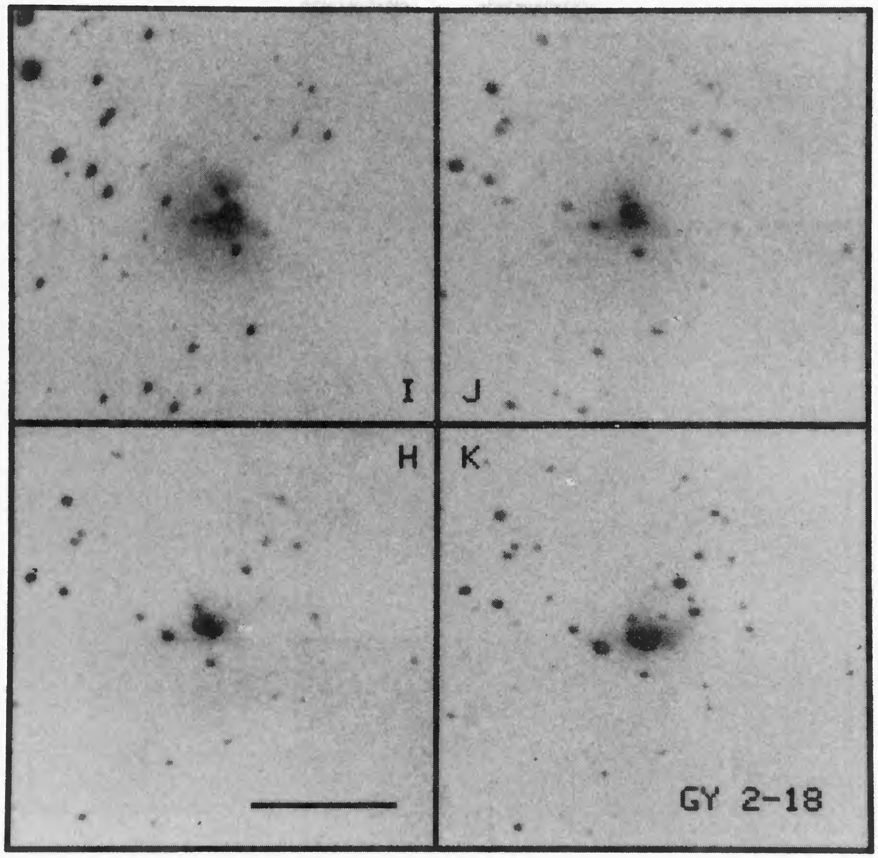

FIG. 7. *IJHK* images of Gy 2-18. North is to the top, east to the left. The length of the bar is 40″.

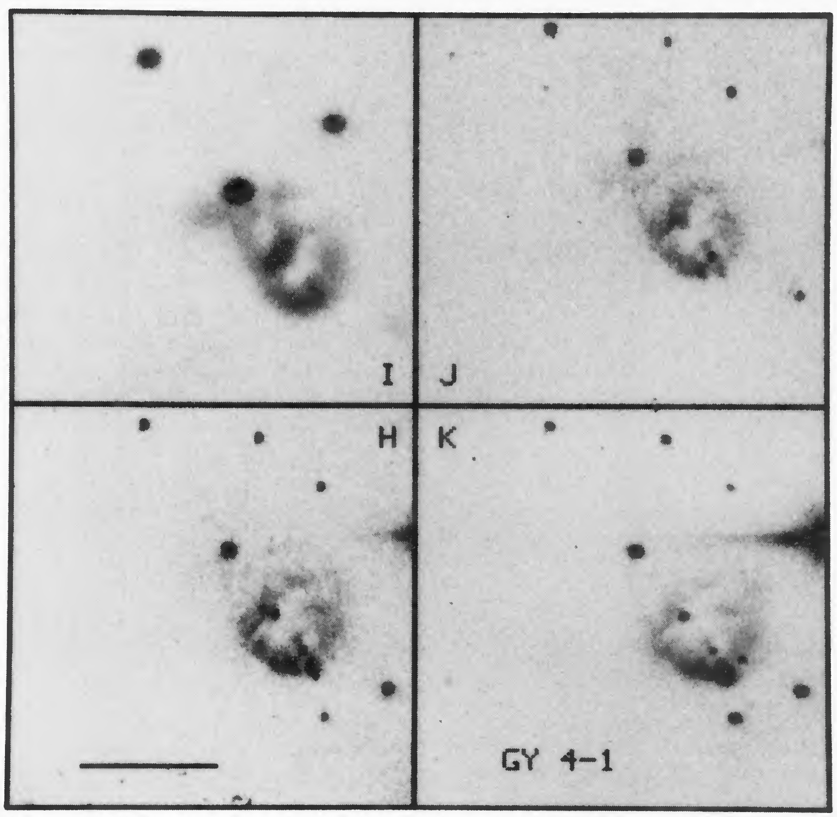

FIG. 8. *IJHK* images of Gy 4-1. North is to the top, east to the left. The length of the bar is 30″.

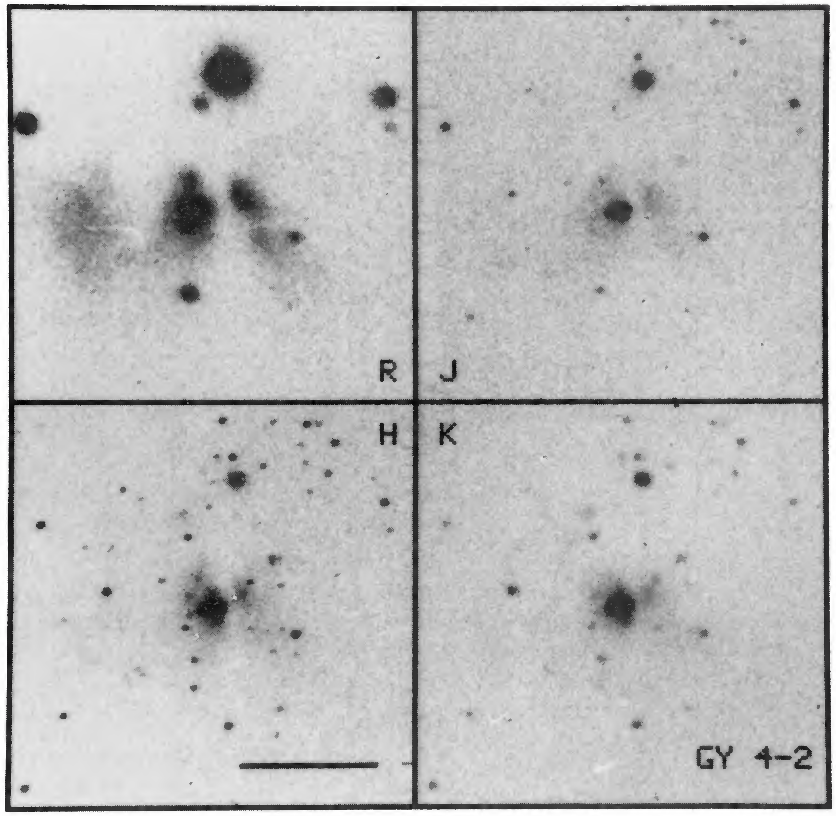

FIG. 9. *RJHK* images of Gy 4-2. North is to the top, east to the left. The length of the bar is 30″.

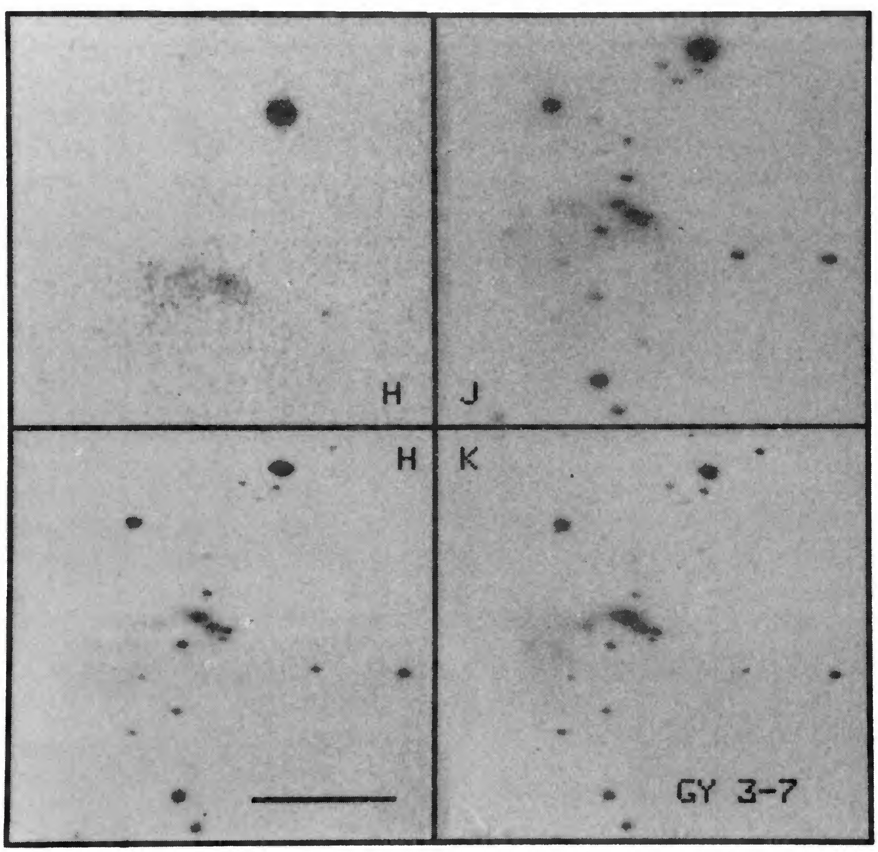

FIG. 10. Hα*JHK* images of Gy 3-7. North is to the top, east to the left. The length of the bar is 30″.

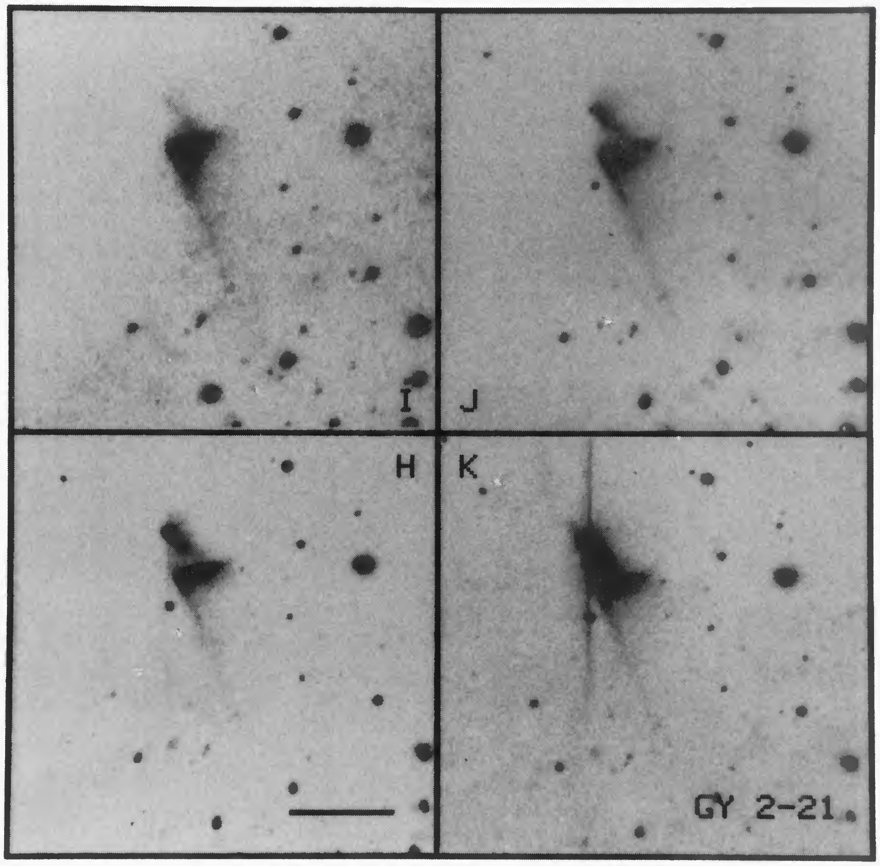

FIG. 11. *IJHK* images of Gy 2-21. North is to the top, east to the left. The length of the bar is 30″.

Gyulbudaghian & Maghakian (1979; GM 1-13), by Parsamian & Petrosian (1979; PP 9), and also listed by Cohen (1980; RNO15). The second centered on the compact far-IR source discovered by Davidson & Jaffe (1984), L1455-FIR, located some 133″ to the NW of PP 9.

Both sources are within the dark cloud L 1455 (Lynds 1962) in Perseus, that is probably associated with the complex NGC 1333 at a distance of 350 pc (Herbig & Jones 1983). This dark cloud is characterized by a dense core traced by NH_3 and CS emission, fragmented in several clumps, the strongest peaking near RNO 15 (Anglada *et al.* 1989; Juan *et al.* 1993). In addition, a high-velocity CO bipolar outflow probably centered on the L1455-FIR was detected by Goldsmith *et al.* (1984) and Levreault (1988a).

RNO 15 is coincident with IRAS 03247+3001. It is associated with an Orion population star (#339 in Herbig & Bell's 1988 catalogue) with $V\simeq 20$ mag (Levreault 1988a) located at its apex. The presence of CO absorption bands in its 2 μm spectrum suggests that its spectral type is K or later (Carr 1989). It also shows Brγ in emission (Carr 1990). The extinction towards this object ($A_V\simeq 8$), as determined by Carr (1990), implies that it lies at the outer part of a dense molecular clump of $\simeq 3.5\ M_\odot$ (Juan *et al.* 1993). The Hα and red continuum narrow-band CCD images suggest that the nebulosity is of a reflection nature. This is confirmed by the fact that the ratio of the stellar flux to that of the SW nebula is 6.4 in both filters. The [S II] image is too noisy for a reliable measurement but seems consistent with this conclusion. As expected, the detailed geometry of the nebula varies with wavelength (Fig. 1); the SW and SE extensions become shorter, opening up at higher angles as wavelength increases. This is best illustrated by the *JHK* "true" color image in Fig. 14 (Plate 38).

Our 3″ aperture *JHK* photometry of RNO 15 centered in the star (Table 3) is consistent with the colors of a reddened ($A_V\simeq 10$) T Tauri star (cf. Fig. 13). The colors of this star, as reported by Evans *et al.* (1986) with an 8″ aperture, are considerably bluer ($K=8.14$, $J-H=1.67$, $H-K=0.83$) compared to ours. The differences are due to the (bluer) contribution of the nebulosity in the larger diaphragm. In fact, we measured $J-H=1.4$, $H-K=0.5$ for the nebula in a 2″ aperture centered some 5″ to the SE of the star.

The source IRAS 03245+3002 corresponds to L1455-FIR (Davidson & Jaffe 1984). Its colors are typical of an embedded core, with an average dust temperature $T_D=42$ K. This very young object lies near the center of one of the dense fragments found in NH_3 and CS by Juan *et al.* (1993) and is associated with an extremely variable H_2O maser (Persi *et al.* 1994). Our *JHK* and H_2 images of L1455-FIR are shown in Fig. 2. At the *IRAS* position we detected a weak source in *K* (#4) that in Hodapp's (1994) deeper *K* image displays a V-shape. This source has also been found by Ladd *et al.* (1993) and Persi *et al.* (1994). From the energy distribution obtained with our near-IR photometry, the *IRAS* data and the flux densities reported by Davidson & Jaffe (1984), we computed a spectral index $n_{2.2-25\mu m} = -3.0$ and a luminosity $L=24L_\odot$. Object #4 is thus, one of the most extreme

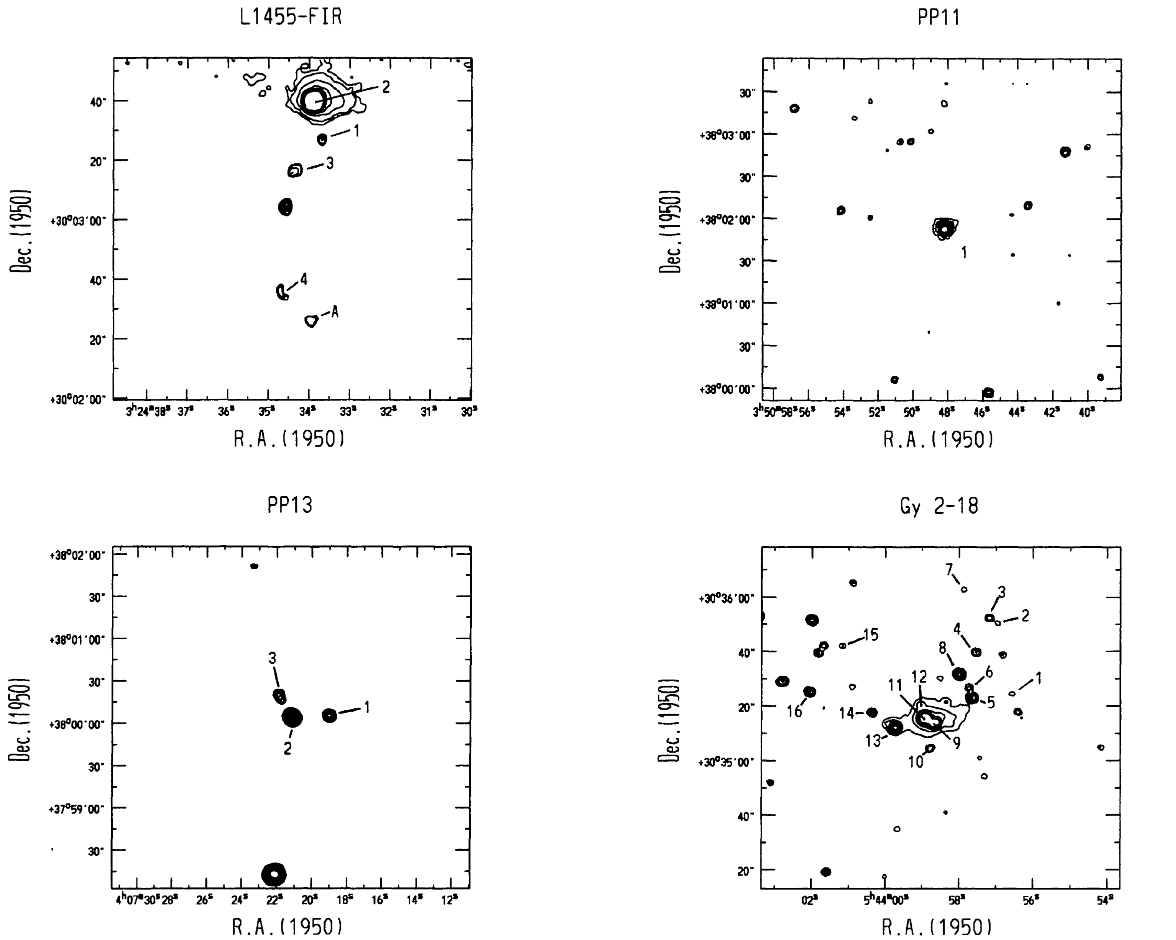

FIG. 12. Identification charts on the contour plots of our K-band images for probable young stellar objects listed in Table 3.

Class I young stellar objects, according to the scheme proposed by Adams *et al.* (1987).

Three other interesting sources (#1, #2, and #3) lie within 1′ to the north of IRAS. Object #1 was detected only in K, while #3 shows colors typical of a reddened T Tauri star. Object #2 seems to be a very highly reddened star ($A_V \simeq 30$) with an associated reflection nebulosity.

Aligned along a straight line to the NW, three knots of H_2 emission appear in the continuum-subtracted 2.12 μm image (Fig. 15). Their coordinates and the H_2 line fluxes are reported in Table 4. Knot A is 10″ SW from the FIR source (#4), while knot C is 220″ to the NE. This kind of aligned systems of reddened shock-excited knots have been also observed in various other regions of NGC 1333 by Hodapp & Ladd (1995). The velocity resolved CO maps by Goldsmith *et al.* (1984) and Levrault (1988a) reveal a complex structure which can be interpreted as indicative of one or more outflows, all of them aligned SE–NW. This contrasts with the observed aforementioned alignement of the H_2 knots and IRAS 03247+3001, which is almost perpendicular to the CO bipolar structures.

3.2 GGD 2 (GM 2-2, HHL 7) and HH 14

This faint and round nebulosity visible in the red Palomar Sky Survey Plate is located near the southern edge of the L1450 (Lynds 1962) dark cloud which includes the very active NGC 1333 complex (cf. Aspin *et al.* 1995; Hodapp & Ladd 1995) close to its center. The position of GGD 2 coincides with IRAS 03254+3050. The *IJHK* images are shown in Fig. 3. Unfortunately, our near-IR images could not be flux calibrated as these were slightly saturated by sky emission, but they clearly indicate that the size of GGD 2 increases with wavelength, (FWHM≃3.5″ at J, 4″ at H, and 5″ at K) suggesting that the emission is probably intrinsic. Ladd *et al.* (1993) report $H-K=1.4$ for this object. The fact that the nebula is also seen in the red and photographic infrared, suggests that its emission does not arise very deep in the cloud. Two other fainter and redder nebular knots appear a few arcsecs to the NW of GGD 2 in the K image. At the distance of 350 pc (Herbig & Jones 1983), the infrared (2–135 μm) luminosity of IRAS 03254+3050 is $2-3L_{\odot}$ (Cohen & Schwartz 1987; Ladd *et al.* 1993), similar to that typical of T Tauri stars. The Hα and [S II] λ6724 emission of GGD 2 is below the detection limit of our CCD images.

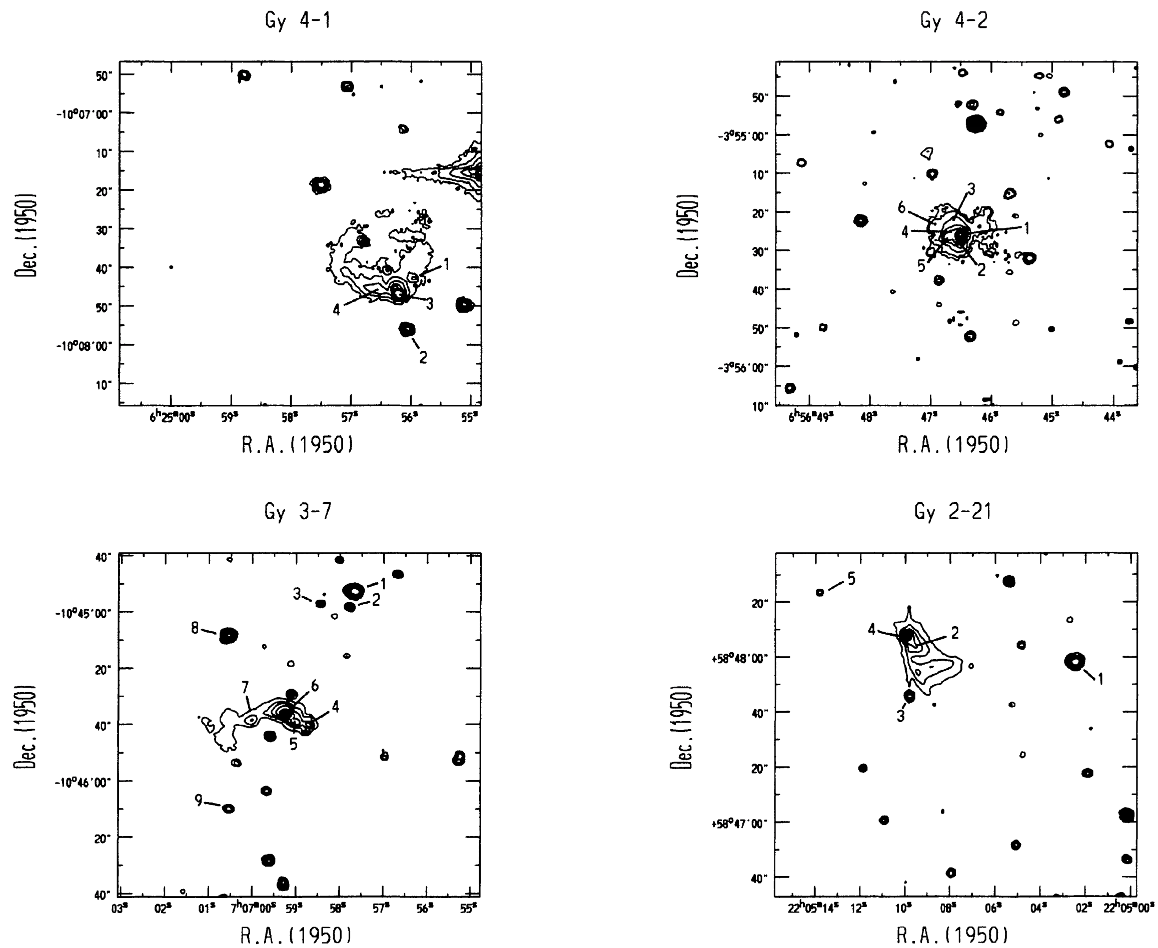

FIG. 12. (continued)

Some 190″ to the east of GGD 2 lies the Herbig-Haro object HH 14. In spite of its complex structure and being in the same cloud as NGC 1333, to our knowledge no detailed studies have been published. In his catalogue, Herbig (1974) describes it as "a group of about 6 nebulous spots" but gives coordinates for only knots HH14B, HH14C, HH14D, and HH14E, which are identified in Fig. 4, where the J, K, continuum-subtracted H_2 and [S II] images are presented. Clearly, the nebulous objects show pure line emission, as no trace of them is seen on the 6250 Å and 2.26 μm continuum filters. The morphology of the knots is similar in Hα and [S II], except that knots C and B are brighter (relative to knot E) in the former. The morphology is similar in molecular hydrogen except that knots C and E are by far the brightest. The 2.12 μm H_2 line flux of each knot is given in Table 4.

Little can be said with the available information about the energy source of this HH complex. The star some 15″ to the NW of knot E is probably a field star ($J-K=1.4$) as it does not show Hα emission and does not appear to show strong excess at 2.2 μm. Cohen & Schwartz (1987) have suggested that IRAS 03254+3050 could be the exciting star of HH 14, but this seems unlikely, considering the probable association of IRAS 03254+3050 with GGD 2 and in view of the complicated geometry required.

3.3 PP 11 (GM 1-14)

PP 11 is a cometary-like nebula with a very faint optical star ($V=21.4$, Levreault 1988a) at its apex and is probably associated with IRAS 03507+3801. CO ($J=1-0$) emission has been detected from this source (Torrelles *et al.* 1983). Searches for molecular outflows and water vapor masers, have been carried out without success by Levreault (1988a) and Persi *et al.* (1994), respectively. Our optical (e.g., R) images show clearly the presence of an arc-shaped reflection nebula which is not observed in the J, H, and K images (Fig. 5). Object #1 (Table 3) is the near-IR counterpart of the optical star and the *IRAS* source. Its energy distribution is typical of a Class II YSO with a very flat far-IR spectrum. From our photometry, we estimated a visual extinction of $A_V=13.4$, and integrating the spectrum from the optical to the far-IR, we obtained a bolometric luminosity $L_{\rm bol}=5.1$ $L_\odot$ assuming a distance of 350 pc (Levreault 1988b). The fact that the optically visible reflection nebula associated with the Class II T-Tau star is not seen in the near-IR, implies that the ambient dust density is not very high in the vicinity of the star, as would be expected for younger (Class I) objects (Tamura *et al.* 1991). The other 10 sources de-

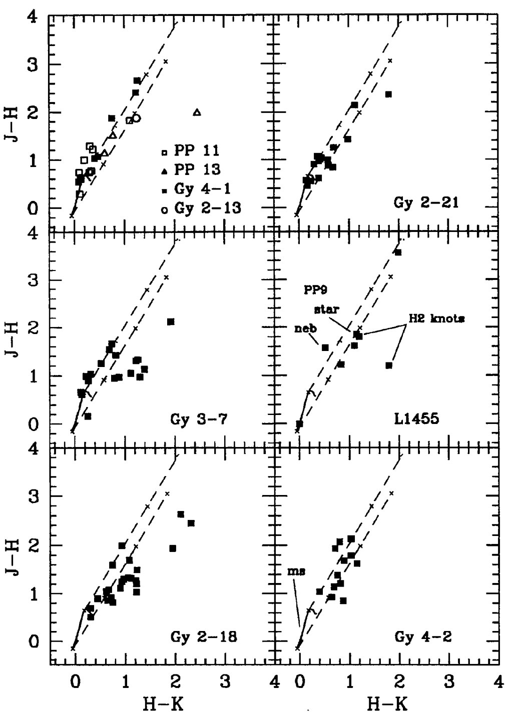

FIG. 13. $J-H$ vs $H-K$ diagrams of all sources measured on our images. The continuous curve (marked ms) indicates the position of the main sequence. The dashed lines are the reddening vectors for late- and early-type stars. Their length corresponds to $A_V=30$.

tected in the $3'\times3'$ field have colors typical of field reddened late-type stars (see color-color plot in Fig. 13).

3.4 PP 13 (Gy 2-10, HHL 13, P 13)

The cometary nebula PP 13 lies within the small dark cloud L 1473, at a kinematic distance of 350 pc from the Sun (Cohen *et al.* 1983). This complex consists of several well separated components, as seen on the *IJHK* images presented in Fig. 6. The northernmost object, PP13N (#3) is an M2.5 T Tauri star (Cohen *et al.* 1983) with a fainter ($\Delta K=1.5$) and redder companion some $\simeq 5''$ to the SW (Smith 1993). PP13S (#2) is a fan-shaped nebula with a low luminosity, highly reddened ($A_V=30-50$) stellar object at its apex (Smith 1993; his Fig. 3). This object shows a spectrum and structure that has been interpreted as a pre-main sequence star of $L_{\rm bol}>30L_\odot$ obscured by a dust disk or torus seen edge-on with an IR reflection nebula (Cohen *et al.* 1983; Smith 1993). The presence of a circumstellar disk has been also suggested by millimeter observations of Osterloh & Beckwith (1995). A fourth stellar object, (#1), previously unstudied, is located some 35″ to the west of PP13S.

We subtracted the continuum frame from our Hα and [S II] images, using two stars more than 50″ away from PP13 as calibrators. The pure Hα and [S II] images show that PP13N and maybe the faint close companion show Hα in emission but none in [S II]. The *JHK* photometry of object #3 = PP13N is consistent with that reported by Cohen *et al.* (1983) and Smith (1993) and implies an $A_V\simeq4$ with a marginal excess at $\lambda>2$ μm. At a distance of 350 pc, the luminosity of PP13N is 0.46 $L_\odot$. The near-IR colors of the westernmost star #1 suggests a similar spectral type to #3 but obscured by an extra three magnitudes in *V* and a negligible near-IR excess. As it also presents evidence of faint [S II] and Hα emission, it may be another pre-main-sequence low-mass star. Optical spectroscopy of this star is required to confirm this.

Our CCD images confirm the puzzling result, first reported by Cohen *et al.* (1983) when discussing their spectroscopic observations, that Hα emission is absent from PP13S, whereas [S II] emission is very prominent. We find that this is valid throughout the nebulosity, which in [S II] is elongated in the SW–NE direction, towards PP13N, as shown in Fig. 16. The high [S II]/Hα ratio provides evidence of shocked gas in PP13S, as suggested by Cohen *et al.* (1983). On the other hand, comparing the K and H_2 images, we exclude any substantial molecular hydrogen emission from PP13S, indicating that the molecular hydrogen has been dissociated. This implies that the shock velocity is >50 km sec^{-1}, as in the case of knot HH1-G (Noriega-Crespo & Garnavich 1994). Cohen *et al.* (1983) also detected metal lines and TiO bands in absorption in the spectrum of PP13S. These may originate in the photosphere of the embedded star and reflected by dust particles in the nebula or caused by *in situ* absorption by material recently ejected from the star above the scattered stellar continuum. At 2.2 μm, the YSO is detected as a point-like source with a roundish nebulosity of size ~14″ and centered 1″ to the west. At shorter wavelengths, only the nebula is seen and its peak emission shifts further away from the star as the wavelength decreases. The maximum observed separation between the star and the peak nebular emission at 6400 Å is 5″. In addition, another nebular protuberance extending some 10″ towards the south of PP13S is present only on our I_c image (Fig. 6) and on the red and blue PSS plates. This seems to be pure reflection, as it is not seen on the narrow-band frames. Thus, PP13S has both reflection and shocked gas emission components: an HH object located physically close to the exciting source, as suggested for RNO 40 by Bohigas *et al.* (1993) and an extended reflection nebula. Based on the available near-IR photometry (Cohen *et al.* 1983; Smith 1993; Manchado *et al.* 1989; Persi *et al.* 1988a and Table 3), object #2 = PP13S seems to be highly variable in the near-IR, amounting to $\Delta K>1.5$. Weintraub & Kastner (1992) reported even greater variability. Such extreme variations are uncommon in T Tauri stars. The *IRAS* source 04073+3800, associated with PP13S, has a probability of variability in the mid-far IR of 82%. The origin of this is unclear at present.

3.5 Gy 2-13 (HHL 17)

Our red and I_c images, shown in Fig. 17, reveal the presence of a very red point-like source associated with an arc-shaped reflection nebula which is not observed in our *JHK* images. The near-IR colors (Fig. 13) combined with the fluxes of IRAS 04591–0856 agree with those expected for a reddened ($A_V\simeq15$) T Tauri star, as had also been suggested by Persi *et al.* (1988b). This source is very similar to PP 11

TABLE 3. Positions and photometry of probable YSO.

Name	α 1950 δ	K	$J-H$	$H-K$	Notes
PP 9					RNO 15
1	$3^h24^m43^s.5+30^\circ01'43''$	9.52	1.85	1.15	IRAS
L1455FIR					
1	$3^h24^m33^s.9+30^\circ03'24''$	15.91	⋯	⋯	
2	$3^h24^m34^s.1+30^\circ03'36''$	10.80	3.56	1.99	Neb.
3	$3^h24^m34^s.5+30^\circ03'14''$	14.92	1.61	1.10	
4	$3^h24^m34^s.6+30^\circ02'36''$	16.00	⋯	1.80	IRAS
Gy 1-4					
1	$3^h50^m48^s.2+38^\circ01'53''$	10.19	1.83	1.10	IRAS
PP 13					
1	$4^h07^m19^s.0+38^\circ00'05''$	9.73	1.50	0.77	
2	$4^h07^m21^s.2+38^\circ00'05''$	8.91	1.98	2.15	PP13S
3	$4^h07^m21^s.9+38^\circ00'20''$	10.29	1.15	0.60	PP13N
Gy 2-13					
1	$4^h59^m06^s.6-8^\circ56'32''$	10.31	1.88	1.24	IRAS
Gy 2-18					
1	$5^h43^m56^s.9+30^\circ35'26''$	14.64	⋯	1.86	
2	$5^h43^m57^s.3+30^\circ35'52''$	14.68	⋯	>1.82	
3	$5^h43^m57^s.5+30^\circ35'53''$	13.87	1.21	1.22	
4	$5^h43^m57^s.9+30^\circ35'41''$	13.56	1.02	1.22	
5	$5^h43^m58^s.0+30^\circ35'25''$	12.78	⋯	3.30	
6	$5^h43^m58^s.0+30^\circ35'28''$	14.27	⋯	>2.20	
7	$5^h43^m58^s.2+30^\circ36'04''$	14.49	⋯	>2.00	
8	$5^h43^m58^s.3+30^\circ35'33''$	12.16	2.63	2.11	IRAS
9	$5^h43^m58^s.9+30^\circ35'16''$	10.33	2.45	2.32	Neb.
10	$5^h43^m59^s.1+30^\circ35'06''$	13.60	0.82	0.65	
11	$5^h43^m59^s.2+30^\circ35'17''$	9.67	1.28	1.21	Neb.
12	$5^h43^m59^s.3+30^\circ35'22''$	13.30	1.31	0.97	
13	$5^h44^m00^s.9+30^\circ35'14''$	11.36	1.94	1.95	
14	$5^h43^m00^s.6+30^\circ35'19''$	13.47	1.34	1.06	
15	$5^h43^m01^s.4+30^\circ35'43''$	14.37	1.50	1.23	
16	$5^h43^m02^s.3+30^\circ35'27''$	12.71	1.33	1.12	
Gy 4-1					
1	$6^h24^m56^s.0-10^\circ07'43''$	14.21	⋯	3.39	
2	$6^h24^m56^s.1-10^\circ07'56''$	12.60	⋯	2.57	
3	$6^h24^m56^s.2-10^\circ07'47''$	11.18	⋯	3.35	IRAS
4	$6^h24^m56^s.5-10^\circ07'46''$	12.86	⋯	1.93	
Gy 4-2					NS14
1	$6^h56^m46^s.5-3^\circ55'26''$	10.47	1.39	0.76	A
2	$6^h56^m46^s.5-3^\circ55'27''$	11.53	1.14	0.69	B
3	$6^h56^m46^s.6-3^\circ55'22''$	11.57	⋯	⋯	
4	$6^h56^m46^s.6-3^\circ55'25''$	12.60	0.85	0.87	D
5	$6^h56^m46^s.7-3^\circ55'27''$	11.68	1.21	0.82	C
6	$6^h56^m46^s.9-3^\circ55'23''$	12.61	⋯	⋯	
Gy3-7					
1	$7^h06^m57^s.6-10^\circ44'53''$	10.17	−0.67	1.89	
2	$7^h06^m57^s.7-10^\circ44'58''$	13.44	1.05	1.12	
3	$7^h06^m58^s.4-10^\circ44'57''$	13.93	0.97	0.88	
4	$7^h06^m58^s.6-10^\circ45'42''$	12.47	1.31	1.22	Neb.
5	$7^h06^m58^s.9-10^\circ45'40''$	11.96	1.33	1.26	Neb.
6	$7^h06^m59^s.2-10^\circ45'36''$	10.91	2.12	1.92	IRAS
7	$7^h06^m00^s.0-10^\circ45'39''$	13.11	1.44	1.95	Neb.
8	$7^h06^m00^s.5-10^\circ45'08''$	11.11	0.97	1.30	
9	$7^h06^m00^s.5-10^\circ46'10''$	13.50	1.13	1.39	
Gy 2-21					
1	$22^h05^m02^s.6+58^\circ47'58''$	10.50	0.84	0.62	
2	$22^h05^m09^s.5+58^\circ48'04''$	12.48	⋯	⋯	Neb.
3	$22^h05^m09^s.8+58^\circ47'46''$	12.91	2.14	1.12	
4	$22^h05^m09^s.9+58^\circ48'08''$	11.27	2.36	1.81	IRAS
5	$22^h05^m13^s.7+58^\circ48'23''$	14.58	1.42	0.98	

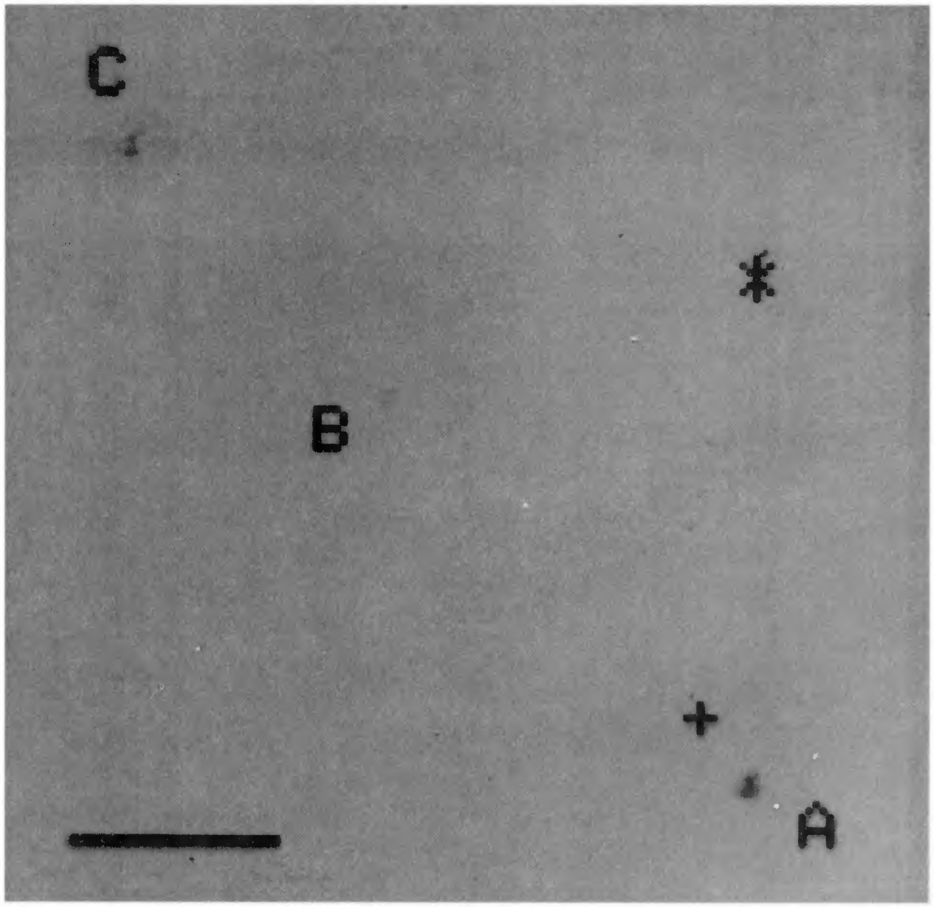

FIG. 15. Continuum subtracted H_2 2.12 μm mosaic of the region near L1455FIR. The H_2 knots are labelled according to Table 4. The plus sign marks the position of IRAS 03245+3002 and the asterisk marks the position of source #2. North is to the top, east to the left. The length of the bar is 30″.

in which the absence of an IR nebula indicates that the ambient dust density is low around the possible class II–III T Tauri star associated with Gy 2-13.

3.6 Gy 2-18 (HHL 31)

This object is located in a dense cloud that has been detected in CO by Wouterloot & Brand (1989) with a radial velocity of -18.5 km s^{-1}, yielding a kinematic distance of 15.6 kpc which, as will be discussed later, is incompatible with the energetics of the sources. In contrast with the Palomar Survey plates which show a mostly nebulous object, our CCD images also reveal a point-like central condensation

TABLE 4. H_2 2.12 μm line fluxes.

Name	α 1950 δ	Flux (10^{-15}erg seg^{-1}cm^{-2})
L1455FIR		
A	$3^h24^m34\overset{s}{.}0+30°02'27''$	1.30
B	$3^h24^m38\overset{s}{.}0+30°03'25''$	0.24
C	$3^h24^m40\overset{s}{.}6+30°03'52''$	0.87
HH14		
B	$3^h25^m45\overset{s}{.}0+30°50'50''$	0.97
C	$3^h25^m44\overset{s}{.}1+30°50'29''$	0.73
D	$3^h25^m44\overset{s}{.}8+30°51'05''$	0.36
E	$3^h25^m44\overset{s}{.}4+30°50'56''$	0.40
F	$3^h25^m44\overset{s}{.}3+30°50'12''$	0.24

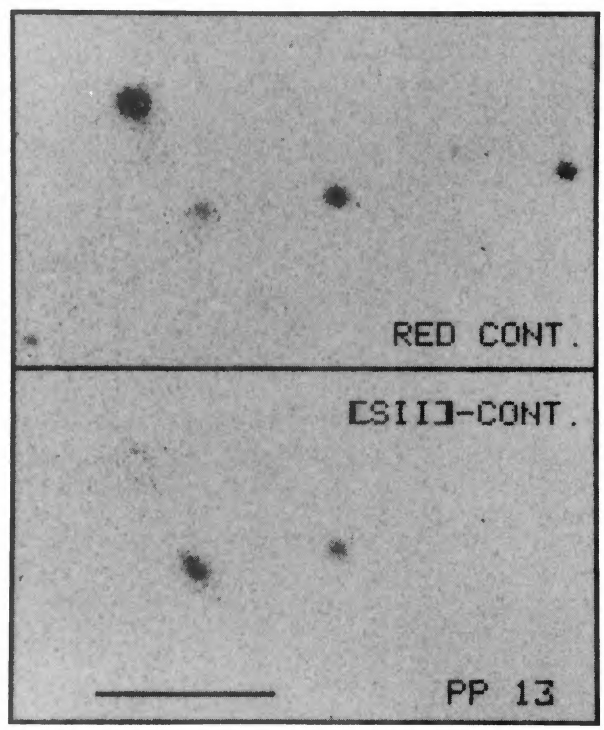

FIG. 16. Red continuum at 6459 Å and continuum subtracted [S II] 6724 Å images of PP 13. North is to the top, east to the left. The length of the bar is 30″.

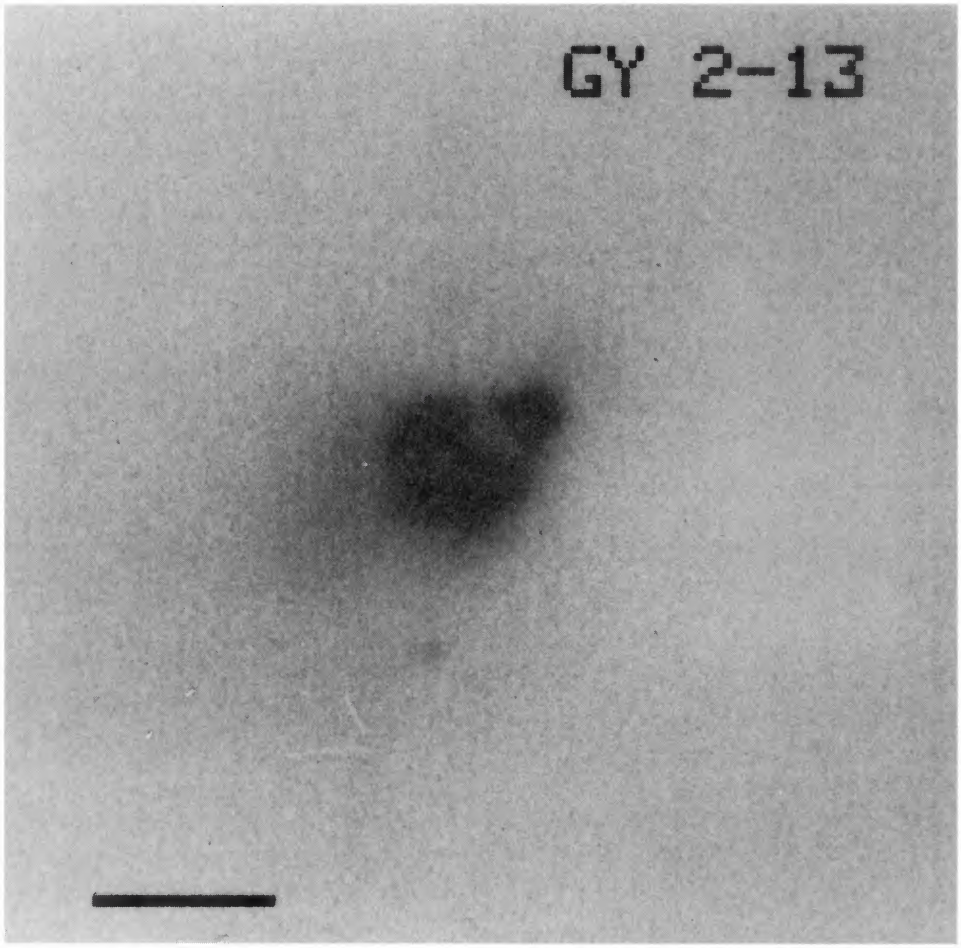

FIG. 17. I_c image of Gy 2-13. North is to the top, east to the left. The length of the bar is 15″.

with a bright Hα in emission, and a faint extended reflection nebula. The *IJHK* images are shown in Fig. 7.

In a field of approximately $2' \times 2'$ centered on IRAS 053439+3035, we detected 31 sources at K, all but two lying within 25″ from the *IRAS* source and in particular #9, 11 and 13 are embedded in the infrared nebula. The $J-H$ versus $H-K$ diagram (Fig. 13) indicates that at least 7 sources (#3, 4, 8, 9, 11, 13, and 15) have IR excesses, whereas objects #5, #6 and #7 were not even detected in J and have $H-K \geqslant 2.2$. Object #9 is the near-infrared counterpart of the *IRAS* source. It was measured photometrically in the near and mid-infrared with a large aperture by Persi *et al.* (1988b) and Campbell *et al.* (1989) who also presented its spectral energy distribution. Their beam included also de bluer object #11 which is a less reddened optically visible young star with Hα emission as discovered on our CCD images. As most of these very red objects are located to the NW of Gy 2-18 (see Fig. 14), we can conclude that the active center of star formation occurs in this area. On the other hand, objects #10, 14, and 16, found to the S and E, have colors of reddened early-type stars (Table 3).

From the position of the probable early type stars (#10, 14, and 16) in the $J-K$ versus $H-K$ diagram, we determined a mean extinction of $A_V \simeq 15$. The best solution for the *IRAS* and the K-band luminosities of most of the probable cluster members and the derived extinction, corresponds to a distance of 3–4 kpc, which implies a total IR luminosity of IRAS 05439+3035 of around $10^4\ L_\odot$, similar to that of a late O-type star which we identify as object #9. Our observations, thus, evince the presence of a young embedded cluster in Gy 2-18 composed by at least 9 very young and massive members ionizing its surrounding H II region.

3.7 Gy 4-1 (HHL 43)

Gy 4-1 is a loop-shaped nebula as illustrated in our I_c image (Fig. 8). The very cold source IRAS 06249−1007 is near the SW tip of this nebulosity. Wilking *et al.* (1989) detected ^{12}CO and ^{13}CO line emission but no strong 2.7 mm, 2 cm, or 6 cm continuum towards this *IRAS* source. The CO line at this position displays high velocity wings implying the possible presence of a bipolar outflow.

Figure 8 shows our *IJHK* images. The nature of Gy 4-1 is clearly that of a reflection nebula. Indeed, no evidence of line emission was found in the Hα, [S II], Brγ and H_2 images when their respective nearby continuum images were subtracted. A displacement is seen in the position of the edges of the nebulosity as the wavelength increases, as can be clearly seen in the ''true color'' image of this object (Fig. 14). The northern loop of Gy 4-1 is much bluer than the southern part of the nebula, implying that the dust density is much lower in the north, further away from the *IRAS* source.

Near the SW edge of the nebula, we found the four sources identified in Fig. 12 to be extremely red with $H-K>2.0$, and too faint at J to be detected (Table 4). The near-IR source #3 is at the nominal position of IRAS 06249–1007, and is the only point-like source present in the L-band image taken at ESO, with $L=6.26$. Integrating the energy distribution and assuming the kinematic distance of 500 pc (Wilking *et al.* 1989), a bolometric luminosity of 290 $L_{\odot}$ is computed. Considering that the *IRAS* beam comprises the four very red sources, it is probable that each component is an embedded T Tauri-type star to account for the total luminosity. The remaining sources in our near-IR images are field stars as shown by their observed near-IR colors (Fig. 13). These are located mainly to the north of the nebula. A preliminary model for this source, pending more detailed observations, i.e., velocity resolved CO high resolution maps, would be that of a multiple system of T Tauri stars powering a bipolar flow, of which only a reflection nebula on the NE lobe can be detected at $\lambda<3$ μm.

3.8 Gy 4-2 (NS 14, HHL 46)

This faint nebula presents a bipolar morphology at almost all wavelengths. It is associated with the source IRAS 06567–0355 (Neckel & Staude 1984), with an expanding ultracompact H II region (Fich 1993) and with a dense and cold molecular cloud (Neckel *et al.* 1989). The nebulosity has a rare combination of both reflection and emission as determined by polarimetric (Scarrott *et al.* 1986) and spectroscopic (Neckel *et al.* 1989) observations.

As part of a comprehensive multiwavelength study of the region, Neckel *et al.* (1989) found an optically visible compact (size 4″) trapezium-type system at the center of the brightest part of the nebulosity. It is composed of four B0.5 to A5 stars, each suffering from substantially different amounts of extinction. These stars provide sufficient energy for heating the dust and ionizing the H II region. The young complex is at a distance of 2.3 kpc (Neckel *et al.* 1989).

The *IJHK* images of NS 14 are presented in Fig. 9. The presence of a small cluster in the vicinity of the trapezium system is clear. The $J-H$ versus $H-K$ diagram of the sources in the field (Fig. 13) shows that approximately half of them, including those belonging to the trapezium, are early-type stars, presumably associated with this young region. Only one (#4 = D in Neckel *et al.* 1989) shows considerable excess at 2 μm and its position in the two-color diagram and luminosity (cf. Neckel *et al.* 1989) suggest that it is a Herbig Ae/Be star. The IR photometry of the other sources in the trapezium shows that these are reddened OB type stars, in agreement with Neckel *et al.* (1989; their Table 1), though our photometry suggests a similar value of $A_V\simeq13$ for stars #5=C, #1=A, and #2=B. The fact that no other star in the scarcely populated cluster presents IR excess, suggests that the cluster and its H II region are in an advanced evolutionary state. Nevertheless, NS14 is associated with a massive molecular cloud of some 1900 $M_{\odot}$ with the trapezium system at its 500 $M_{\odot}$ core (Neckel *et al.* 1989).

3.9 Gy 3-7 (HHL 49)

Gy 3-7 is associated with the high luminosity *IRAS* source 07069–1045. From their CO observations, Wouterloot & Brand (1989) report a kinematic distance of 1.41 kpc to the object. No water maser has been found in the vicinity of the *IRAS* source (Palla *et al.* 1991).

The observed emission in Hα extends some 20″ in the E–W direction with two lobes, the brightest and westernmost of which lies between objects #4 and #5 and a fainter source with $K=13.35$, $J-K=0.95$, and $H-K=0.79$ which is located 2″ to the SE of #4. (see Fig. 12). [S II] is very faint leading to the conclusion that the nebula is photoionized. In the near-IR, particularly in K, this nebula extends further 16″ to the SE (see Fig. 10).

The photometric results (see the two-color diagram in Fig. 13) reveal four sources (#4, 5, 6, and 7) located within a radius of 8″ which show strong IR excesses. Source #6 is at the position of the *IRAS* source and was also detected in our L-band image ($L=7.86\pm0.11$). These young stars form the core of a small cluster powering the H II region. Assuming the kinematic distance of 1.41 kpc, the total luminosity of the *IRAS* source, is 1.2×10^3 $L_{\odot}$ which is too low for a star responsible for the ionization of the H II region (i.e., of spectral type earlier than B2). Therefore, the distance to Gy 3-7 should be at least a factor of two larger. Other sources with a significant IR excesses (#2, #3, and #8) lie about 30″–40″ north of the nebula, and their relation to GY 3-7 and IRAS 07069–1045 should be investigated further.

3.10 Gy 2-21 (HHL 75)

This object is located on a sharp edge of the dark cloud L1165 (Lynds 1962). In the optical, it resembles a boomerang with a long "cometary" tail towards one side. The *IRAS* point source 22051+5848 is located some 20″ to the NW of the optical brightest nebula. The *IRAS* colors are typical of embedded cores (e.g., Parker 1991). Assuming a kinematic distance to L1165 of 200 pc, the infrared luminosity is $L_{1-100\mu m}=4$ $L_{\odot}$ (Persi *et al.* 1988a) and the bolometric luminosity $L_{\rm bol}\simeq9$ $L_{\odot}$ (Schwartz *et al.* 1991). In spite of the uncertainty in the distance to Gy 2-21, the presence of an embedded T Tauri star can be safely inferred. A ^{12}CO $J=2\rightarrow1$ survey by Parker *et al.* (1991) revealed a well defined bipolar outflow, with peaks of blue and redshifted emission some 20″ to the north and south of the *IRAS* source. No H_2O maser source was detected in the vicinity of Gy 2-21 in the survey by Persi *et al.* (1994).

Figure 11 shows the *IJHK* broad-band images. The near-IR frames are combined in the "true" color image presented in Fig. 14. Analyses of all images revealed the following characteristics of this region:

(a) A nebulosity with the shape of a scythe is seen at all wavelengths, from the 0.6 to 2.2 μm, with the width of its knife and the length of its pole diminishing as the wavelength increases. Subtracting the continuum from the narrow-band images revealed that no Hα or H_2 emission is present, indicating that Gy 2-21 is a reflection nebulosity, albeit with a peculiar shape. This is supported by the *JHK*

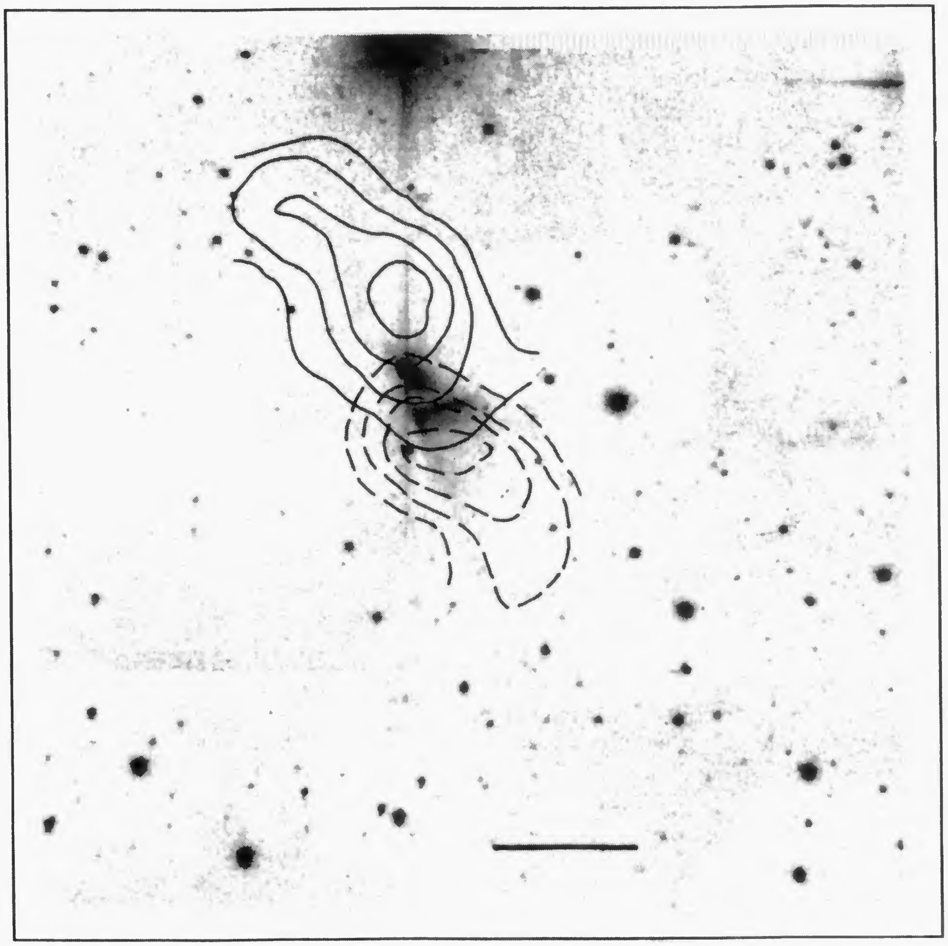

FIG. 18. Contour plots of the CO blue (continuous line) and red (broken line) lobes of the bipolar flow centered on IRAS 22051+5848 (Gy 2-21) superposed on our K-band mosaic. North is to the top, east to the left. The length of the bar is 40″.

colors of the nebulosity, which are similar to those of a late-type photosphere reddened by $A_V=3-4$.

(b) Within 2″ of the *IRAS* nominal position, a point-like near-IR source (#4) with no optical counterpart was found. Its *JHK* photometry is that of a very young core object and therefore, we identify this as the near-IR counterpart of the *IRAS* source. An elongated protuberance (object #2) of length ~7″ pointing towards the visible scythe-shaped nebula emanating from the stellar object is also seen in all broad-band colors with no appreciable molecular hydrogen emission. The IR complex source is located precisely at the center of the CO bipolar flow (Parker *et al.* 1991). This is illustrated in Fig. 18, where the blue and redshifted wings of the ^{12}CO line emission are plotted superposed on the grey-scaled K image. This clearly indicates that the *IRAS* and near-IR source is the driving source of the outflow. The implied geometry of the outflow is *sui generis*; the blueshifted lobe, normally coincident with the region of lowest obscuration as this lobe is approaching the observer, occurs here in the region of highest obscuration, near the center of the L1165 dark cloud. This is confirmed by two facts: that the optically visible reflection nebulosity is seen on the southern, redshifted lobe and that most of this CO lobe extends to the outside of the well delimitted dark cloud (cf. blue and red Palomar Survey Plates).

(c) The location on the $J-H$ versus $H-K$ diagram of the point-like sources (Fig. 13) revealed that most are reddened field late-type stars, with the possible exception of objects #1 and #5 which could be reddened ($A_V=10-15$) early-type stars. The latter well embedded in the dark cloud. Object #3, located very close to the reflection nebula and near the center of the red CO lobe, has colors typical of a reddened ($A_V=14-16$) late-type, most probably a background star.

(d) A very red ($I-K>10$) and bright at ($K<9$) point-like source is located some 90″ to the north of Gy 2-21 and coincides with the position of *IRAS* 22051+5849, but its *IRAS* (12 and 25 μm) color corresponds to a blackbody at $T>1000$ K. No accurate K photometry was obtained for this source as it is at the edge of our mosaic.

4. CONCLUSIONS

During the course of this study, we have performed a morphological and photometric study of a sample of eleven regions characterized by the presence of small red nebulosities in dusty environments which have associated *IRAS* sources with 12–100 μm colors of pre-main-sequence objects. Although in appearance the sample looked homogeneous, the results here obtained imply a large variety of physical conditions applicable to each object. As expected, these depend mostly, but not uniquely, on the mass of the YSO as well as its evolutionary status.

TABLE 5. Characteristics of the studied regions.

Name	IRAS	Dist. (kpc)	Lum. $L_{\odot}$	Ref. Lum.	Dark cloud	YSO class	A_V	Neb. opt.	Neb. IR	Notes
PP 9	03247+3001	0.35	8	1	L1455	II-III	9	R	R	b
L1455FIR	03245+3002	0.35	24	0	L1455	I	>20	no	S	b
GGD 2	03254+3050	0.35	3	2	L1450	···	···	?	?	···
PP 11	03507+3801	0.35	5	0		II	13.4	R	no	···
PP 13	04073+3800	0.35	32	4	L1473	I	>30	S,R	R	m
Gy 2-13	04591−0856	0.54	7	3		II	15	R	no	···
Gy 2-18	05439+3035	3.50	10^4	0		O-B0	15	P	P	c
Gy 4-1	06249−1007	0.50	290	0		I	>22	R	R	b,m
Gy 4-2	06567−0355	2.30	10^4	5	BFS57	B0	13	P	P	c
Gy 3-7	07069−1045	>1.40	$>10^3$	0		B1-B5	15	P	P,R?	c
Gy 2-21	22051+5848	0.20	9	3	L1165	I	>15	R	R	b,m

Notes to TABLE 5

R: Reflection, S: Shocked, P:Photoionized, b: CO bipolar flow, c: cluster, m: multiple.

References to TABLE 5

(0) This work; (1) Evans *et al.* 1986; (2) Ladd *et al.* 1993; (3) Persi *et al.* 1994; (4) Cohen *et al.* 1983; (5) Neckel *et al.* 1989.

In all cases, the association between the nebulous objects, the *IRAS* sources and the near-infrared counterparts is confirmed. In Table 5 we present the summary of the results. For each nebula, the name of the *IRAS* source and associated dark cloud is indicated. In most cases, the distance to the complexes were taken from the literature, though for some, these were re-evaluated as their kinematic distances were incompatible with the respective photometry and energetics. The total luminosity of the objects are given with their reference. Following the criteria proposed by Adams *et al.* (1987), the evolutionary class of low and intermediate mass YSO are assigned to each source. For each of the most luminous objects, a range of probable spectral types is determined. A_V was estimated from the $J-H$ versus $H-K$ diagram and other criteria, when possible. The nature (photoionized, shock-excited or reflection) of both the optical and near infrared nebula is indicated.

The most luminous sources ($L > 10^3\ L_{\odot}$) are each associated with a cluster of early-type stars and an H II region. In the case of the younger regions (Gy 2-18 and Gy 3-7), a large fraction of the embedded objects display significant IR excesses, while the most evolved one (Gy 4-2) is optically visible without IR excess emission.

Optical and infrared reflection nebulae have been detected in the Class I low luminosity YSOs in the dark clouds L1455, L1473, and L1165 as well as in Gy 4-1. These objects are all associated with high-velocity CO bipolar outflows, confirming the conclusion by Tamura *et al.* (1991) that the presence of near-IR nebulosities is indicative of circumstellar dust disks and mass outflows from the very young embedded sources. Three of the nebulosities, PP 9, Gy 4-1, and Gy 2-21 display a reflection nebula but no evidence of shock excitation in spite of the presence of bipolar outflows. In the more evolved low mass objects PP 11 and Gy 2-13 here classified as Class II–III sources, no infrared nebula was detected, although they have optical reflection nebula.

We thank Dr. Miguel Roth for help with the LCO observations. This work was supported by grants from CONACyT-CNR and DGAPA-UNAM (IN-108696). We made extensive use of the SIMBAD database, operated at CDS, Strasbourg, France. Support from the technical staff of all observatories involved is acknowledged.

REFERENCES

Adams, F. C., Lada, C. J., & Shu, F. H. 1987, ApJ, 312, 788
André, P. 1994, in The Cold Universe, XXVIII Recontre de Morion, edited by Th. Montmerle *et al.* (Editions Frontières), p. 179
Anglada, G., Rodríguez, L. F., Torrelles, J. M., Estatella, R., Ho, P. T. P., Cantó, J., López, R., & Verdes-Montenegro, L. 1989, ApJ, 341, 208
Aspin, C., Sandell, G., & Russell, A. P. G. 1995, A&AS, 106, 165
Bohigas, J., Persi, P., & Tapia, M. 1993, A&A, 267, 168
Campbell, B., Persson, S. E., & Mathews, K. 1989, AJ, 98, 643
Cantó, J. 1981, in Investigating the Universe, edited by F. D. Kahn (Reidel, Dordrecht), p. 95
Carr, J. S. 1989, ApJ, 345, 522
Carr, J. S. 1990, AJ, 100, 1244
Cohen, M. 1980, AJ, 85, 29
Cohen, M., & Schwartz, R. D. 1987, ApJ, 316, 311
Cohen, M., Aitken, D. K., Roche, P. F., & Williams, P. M. 1983, ApJ, 273, 624
Cruz-González, I., *et al.* 1994, Proc. SPIE Astron. Instrum., 8, 199
Davidson, J. A., & Jaffe, D. T. 1984, ApJ, 277, L13
Elias, J. H., Frogel, J. A., Matthews, K., & Neugebauer, G. 1982, AJ, 87, 1029
Evans, N. J., Levreault, R. M., & Harvey, P. M. 1986, ApJ, 301, 894
Fich, M. 1993, ApJS, 86, 475
Goldsmith, P. F., Snell, R. F., Hemeon-Heyer, M., & Langer, W. D. 1984, ApJ, 285, 599
Gyulbudaghian, A. L. 1983, Pis'ma Astron. Zh., 8, 222 (Sov. Astron. Lett., 8, 123)
Gyulbudaghian, A. L. 1984a, Astrofizika, 20, 631
Gyulbudaghian, A. L. 1984b, Astron. Tsirk., 1342,
Gyulbudaghian, A. L., & Maghakian, T. Y. 1979, Pis'ma Astron. Zh., 3, 232 (Sov. Astron. Lett., 3, 58)
Gyulbudaghian, A. L., Glushkov, Yu J., & Denisyuk, E. K. 1978, ApJ, 224, L137
Gyulbudaghian, A. L., Rodríguez, L. F., & Mendoza-Torres, E. 1987, RMxA&A 15, 53

Hartigan, P., Raymond, J., & Hartmann, L. 1987, ApJ, 316, 232
Herbig, G. H. 1974, Lick Obs. Bull., 658,
Herbig, G. H., & Bell, K. R. 1988, Lick Obs. Bull. , 1111,
Herbig, G. H., & Jones, B. F. 1983, AJ, 88, 1040
Hodapp, C. W. 1994, ApJS, 94, 615
Hodapp, C. W., & Ladd, E. F. 1995, ApJ, 453, 715
Juan, J., Bachiller, R., Kömpe, C., & Martín-Pintado, J. 1993, A&A, 270, 432
Ladd, E. F., Lada, E. A., & Myers, P. C. 1993, ApJ, 410, 168
Levreault, R. M. 1988a, ApJS, 67, 283
Levreault, R. M. 1988b, ApJ, 897, 910
Lisi, F., *et al.* 1996, PASP, 108, 364
Lynds, B. T. 1962, ApJS, 7, 1
Manchado, A., Pottasch, S. R., García-Lario, P., Esteban, C., & Mampaso, A. 1989, A&A 214, 139
Neckel, T., & Staude, H. J. 1984, A&A, 131, 200
Neckel, T., Staude, H. J., Meisenheimer, K., Chini, R., & Gusten, R. 1989, A&A, 210, 378
Noriega-Crespo, A., & Garnavich, P. M. 1994, RMxA&A 28, 173
Osterloh, M., & Beckwith, S. V. W. 1995, ApJ, 439, 288
Palla, F., Brand, J., Cesaroni, R., Comoretto, G., & Felli, M. 1991, A&A, 246, 249
Parker, N. D. 1991, MNRAS, 252, 63
Parker, N. D., Padman, R., & Scott, P. F. 1991, MNRAS, 252, 442
Parsamian, E. S., & Petrosian, V. M. 1979, Soobshenia Byurakanskoi Obs. Akad. Nauk. Armianskoi S.S.R., No. 51
Persi, P., Ferrari-Toniolo, M., Busso, M., Robberto, M., Scaltriti, F., & Silvestro, G. 1988a, AJ, 95, 1167
Persi, P., Busso, M., Ferrari-Toniolo, M., Marenzi, A. R. 1988b, in Mass Outflows from stars and Galactic Nuclei, edited by L. Bianchi and R. Gilmozzi (Kluwer, Dordrecht), p. 337
Persi, P., Palagi, F., & Felli, M. 1994, A&A, 291, 577
Persson, S. E., West, S. C., Carr, D. M., Sivaramakrishnan, A., & Morphey, D. C. 1992, PASP, 104, 204
Salas, L., *et al.* 1996, Appl. Opt. (in press)
Scarrott, S. M., Brosch, N., Ward-Thompson, D., & Warren-Smith, R. F. 1986, MNRAS, 223, 505
Schwartz, R. D., Gyulbudaghian, A. L., & Wilking, B. A. 1991, ApJ, 370, 263
Smith, R. G. 1993, MNRAS, 264, 587
Stetson, P. B. 1987, PASP, 99, 191
Tamura, M., Gatley, I., Waller, W., & Werner, M. W. 1991, ApJ, 374, L25
Torrelles, J. M., Rodríguez, L. F., Cantó, J., Marcaide, J., & Gyulbudaghian, A. L. 1983, RMxA&A 8, 147
Weintraub, D. A., & Kastner, J. H. 1992, BAAS, 24, 1141
Wilking, B. A., Mundy, L. G., Blackwell, J. H., & Howe, J. E. 1989, ApJ, 345, 257
Wouterloot, J. G. A., & Brand, J. 1989, A&AS, 80, 149

FIG. 14. "True color" images of PP 9, Gy 2-21, Gy 4-1 and Gy 2-18 made from the *J* (blue), *H* (green) and *K* (red) individual frames. North is to the top, east to the left.

Tapia *et al.* (see page 1777)